

# Archangel: A Hybrid UAV-based Human Detection Benchmark with Position and Pose Metadata

Yi-Ting Shen, Yaesop Lee, Heesung Kwon, Damon M. Conover, Shuvra S. Bhattacharyya, Nikolas Vale, Joshua D. Gray, G. Jeremy Leong, Kenneth Evensen, Frank Skirlo

**Abstract**—Learning to detect objects, such as humans, in imagery captured by an unmanned aerial vehicle (UAV) usually suffers from tremendous variations caused by the UAV’s position towards the objects. In addition, existing UAV-based benchmark datasets do not provide adequate dataset metadata, which is essential for precise model diagnosis and learning features invariant to those variations. In this paper, we introduce *Archangel*, the first UAV-based object detection dataset composed of real and synthetic subsets captured with similar imaging conditions and UAV position and object pose metadata. A series of experiments are carefully designed with a state-of-the-art object detector to demonstrate the benefits of leveraging the metadata during model evaluation. Moreover, several crucial insights involving both real and synthetic data during model fine-tuning are presented. In the end, we discuss the advantages, limitations, and future directions regarding *Archangel* to highlight its distinct value for the broader machine learning community.

**Index Terms**—UAV-based object detection, Human detection, UAV-based benchmark dataset, Position metadata, Synthetic data, Model optimization

## I. INTRODUCTION

WITH the recent rapid advancement in edge computing technology coupled with resource-constrained mobile platforms, particularly unmanned aerial vehicles (UAVs) with electro-optical (EO) sensor payloads, a wide range of UAV-enabled applications have been more prevalent. Notable examples include UAV-enabled search and rescue in disaster management [13], aerial surveillance and reconnaissance for civilian and military purposes [1], precision agriculture [51], traffic analysis [22], and intelligent transportation applications [34]. Lately, owing to the remarkable progress of artificial intelligence and machine learning (AI/ML) technology, tailored to distinct constraints of small UAV platforms, these UAV-based applications have been frequently providing promising solutions and successfully achieving the goals and operational requirements of their corresponding applications. Central to the above UAV-based applications are streamlined AI/ML

plug-ins that can effectively interrogate real-time imagery, captured with UAVs, and provide image/video analytics relevant to UAV-based scene understanding, particularly object detection and recognition.

Recently, extensive efforts in object detection and recognition have led to extraordinary advances in the perception accuracy in various challenges associated with large-scale object detection benchmarks that were captured primarily with ground-based cameras [9], [14], [28]. Compared to ground-based object detection and recognition, UAV-based object detection poses unique and severe challenges, as UAV flight inevitably results in a wider range of variations in the conditions for capturing images, including the altitudes and viewing angles of cameras, system turbulence, and weather events. These variations lead to more drastic variations in object appearances/attributes, and thus pose additional challenges to onboard detection models in the location and recognition of objects of interest. In general, changes in object appearances/attributes, caused by varying the image collection conditions, entail three major dependencies: (1) pose dependency caused by changes in the UAV position or camera viewing angle, (2) scale dependency owing to the distance between the UAV and object, and (3) image quality dependency due to UAV turbulence or various weather conditions.

We argue that developing object detection models which can adequately learn features invariant to these dependencies is key to substantially enhancing object detection accuracy in UAV-based perception. This requires curating UAV-based datasets that include images and metadata that carefully depict the full spectrum of correlations between the target scene on the ground and the camera on the UAV, whose imaging conditions constantly change as the UAV navigates the entire range of given operational requirements. Therefore, it is imperative to have a UAV-based object detection benchmark carefully curated with object poses, UAV positions, and weather information in the form of metadata for accurate model validation and verification.

Existing UAV-based benchmarks, such as VisDrone [56], UAVDT [52], Okutama-Action [3], and Standford Drone Dataset [38], provide limited metadata. Despite containing a wide variety of scenes captured using UAVs under different circumstances with various types of objects of interest, they do not provide a complete set of metadata, such as object poses and UAV positions, for each image across the whole datasets. This significant lack of information about how objects on the ground are projected through the camera lens as a function of UAV positions can lead to considerable limita-

Y. Shen, Y. Lee and S. S. Bhattacharyya are with University of Maryland, ECE Department and UMIACS, College Park, MD. (email: ytshen@umd.edu, yaesop@terpmail.umd.edu, ssb@umd.edu).

H. Kwon, D. M. Conover and N. Vale are with DEVCOM Army Research Laboratory (ARL), Adelphi, MD. (email: {heesung.kwon.civ, damon.m.conover.civ, nikolas.g.vale.civ}@army.mil)

J. D. Gray is with Fibertek Inc., Herndon, VA. (email: joshua.d.gray49.ctr@army.mil)

G. J. Leong is with Department of Energy, Washington, DC. (email: g.jeremy.leong@gmail.com)

K. Evensen and F. Skirlo are with Defense Threat Reduction Agency (DTRA), Fort Belvoir, VA. (email: {kenneth.c.evensen.civ, frank.e.skirlo.ctr}@mail.mil)

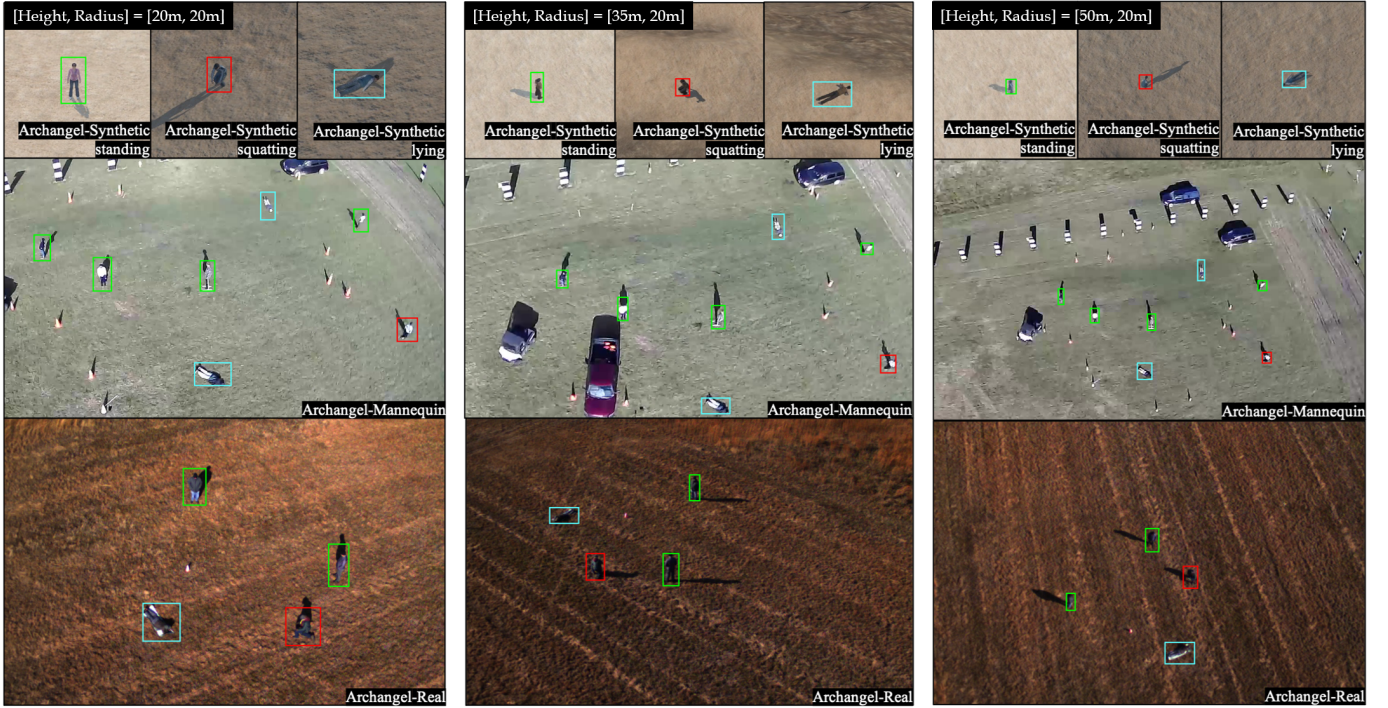


Fig. 1. Examples of images in *Archangel-Synthetic* (top), *Archangel-Mannequin* (middle), and *Archangel-Real* (bottom). Each image is labeled with its corresponding UAV position [Height, Radius]: [20m, 20m] (left), [35m, 20m] (middle), and [50m, 20m] (right). Each instance is labelled with its corresponding object pose: *stand* (green), *squat* or *kneel* (red), and *prone* (cyan).

tions in learning about the objects in UAV-based images, as the appearances/attributes of the objects are subject to large variations.

To overcome the limitation resulting from lack of meta-data, we introduce a large-scale UAV-based dataset, called *Archangel*, collected with comprehensive position and pose information by the DEVCOM Army Research Laboratory (ARL) (Fig. 1). *Archangel* comprises three sub-datasets: *Archangel-Real* [25], *Archangel-Mannequin* [25], and *Archangel-Synthetic* [24]. *Archangel-Real* comprises video sequences captured by a UAV flying at various altitudes and radii of rotation circles. It sets a group of real humans as targets, and each human is in one of three possible poses (*stand*, *kneel* or *squat*<sup>1</sup>, and *prone*) (Fig. 2). Similarly, *Archangel-Mannequin* sets a group of mannequins and different types of vehicles as targets. The imaging conditions for these two sub-datasets, such as UAV altitudes, ranges to targets, and object poses, are the same. Unlike *Archangel-Real* and *Archangel-Mannequin*, which are collected in real-world environments, *Archangel-Synthetic* is generated using the Unity game engine [19]. It includes a number of different virtual characters, who are in the same poses as described above and rendered with diverse illumination conditions. *Archangel-Synthetic* is designed to augment the other two real sub-datasets and for studying various issues tied to optimizing ML models using synthetic data, such as synthetic data augmentation and domain adaptation [37], with respect to UAV-based scene understanding.



Fig. 2. Examples of the three poses in *Archangel*: *stand* (left), *squat* or *kneel* (middle), and *prone* (right).

In addition to collecting a new dataset, we further characterize *Archangel* using state-of-the-art (SoTA) object detection models, specifically the YOLOv5 family [18] which has five different levels of architectural complexity and is pre-trained on MS-COCO [28], a large-scale ground-based object detection dataset. In this paper, we focus on the YOLOv5 models with lower complexity (*YOLOv5n6*, *YOLOv5s6*, *YOLOv5m6*) since they are able to run on computing resource typically available on small UAV platforms (Tab. II). For each model, we evaluate its human detection performance using *Archangel-Real*. Since we programmed our UAVs to circle around the human targets at various altitudes and radii during data collection (Fig. 3), the detection accuracy can be

<sup>1</sup>The terms *kneel* and *squat* are used interchangeably throughout this paper.

compared across the whole range of UAV positions (Sec. V-C).

Furthermore, we optimize the pre-trained YOLOv5 models with different fine-tuning strategies using various hybrid combinations of subsets from *Archangel-Mannequin* and *Archangel-Synthetic*. These fine-tuning strategies have been designed to provide valuable guidelines for leveraging synthetic data in training ML models to boost their performance. A comprehensive performance comparison between the baseline and the optimized YOLOv5 models is presented to demonstrate how incorporating a combination of real and synthetic data can enhance detection performance across varying UAV positions (Sec. IV and V). One of the critical findings from the comparative performance analysis indicates that if the real and synthetic data used for fine-tuning is balanced with respect to the amount of data, a significant performance boost can be achieved even with a low-complexity model, such as *YOLOv5n6* (Sec. V-A). Furthermore, the optimization based on the real and synthetic data is much more effective on infrequent object poses that are rarely seen in the original dataset for pre-training. For example, *prone* from *Archangel* is not often seen in MS-COCO [28], so the performance improvement on this pose is more evident (Sec. V-B).

This paper is extended from our previous preliminary studies [24], [25], where we mainly focus on introducing and characterizing new datasets **separately**. As a result, the major scope of this paper is to **jointly** study the three sub-datasets as a unified UAV-based benchmark with metadata for human detection. In summary, the contributions of this paper are as follows:

- 1) We present a unified *Archangel* dataset<sup>2</sup> after substantially restructuring the three sub-datasets since our conference publications [25], [24], including additional labeling *Archangel-Real* and an expansion of the range of *Archangel-Synthetic*. To the best of our knowledge, *Archangel* is the first UAV-based object detection dataset which contains real and synthetic sub-datasets captured with similar imaging conditions and includes an extensive set of metadata (object poses and UAV positions).
- 2) We conduct extensive data analysis on *Archangel* by jointly analyzing its three sub-datasets (*Archangel-Synthetic*, *Archangel-Mannequin*, and *Archangel-Real*). In particular, we provide several important guidelines on exploiting real and synthetic data together to improve UAV-based object detectors.

## II. RELATED WORK

### A. UAV-based Object Detection Datasets

There is an increasing number of large-scale benchmarks for object detection, utilizing images captured with some fixed or moving cameras on the ground [28], [14], [23], [41], [11], [15], [40], yet relatively few datasets have been collected with UAVs. VisDrone [56] and VisDrone-Challenge [8] is one of the major datasets and challenges for UAV-based object detection. It consists of images captured with UAVs in dozens of different scenarios, in which 10 categories of objects are selected and

carefully labelled. While it does have an advantage in data diversity, VisDrone does not provide any metadata, such as UAV positions. In contrast to VisDrone, UAVDT [52], another well-known benchmark for UAV-based detection and tracking, provides three different kinds of UAV-specific metadata (weather condition, flying altitude, and viewing angle) and a few object attributes such as vehicle category. However, the annotations for the metadata are coarse (3 categories for each). Also, the dataset does not contain the human category. Unlike UAVDT, Okutama-Action [3] is composed of images from aerial views and contains humans in different human poses. However, it provides limited metadata regarding UAV altitudes and camera viewing angles. More recently, A212-Haze [36], which is used in the recent *UG<sup>2</sup>+ Challenge* [44], is the first real haze and object detection dataset with in-situ smoke measurements aligned to aerial imagery. While their goal is to assist research on the interaction between UAV-based object detection and image enhancement/restoration, the goal of our *Archangel* is to facilitate studies on how to improve UAV-based object detectors by using different types of metadata or synthetic data.

There are two other types of datasets which are closely related to UAV-based object detection. First, datasets such as DOTA [10] include aerial images collected from satellites or aircraft. Although they are usually curated for remote sensing applications, detecting objects in such datasets also suffers from severe variations in the scale and orientation of the objects. Second, some UAV-based datasets are designed for certain vision tasks strongly associated with object detection. For instance, CARPK [16] is a large-scale car parking lot dataset designed for object counting. MOR-UAV [33] is a large-scale moving object recognition dataset comprising videos captured by a UAV in various environments, such as urban areas and highways. Stanford Drone Dataset [38] is used for analyzing various object trajectories in the real world from the top-view. UAV123 [35] is used for low altitude UAV-based object tracking. Similar to *Archangel*, UAV123 also includes synthetic data generated by a photo-realistic simulator.

A comprehensive investigation of recent UAV-based datasets is shown in Tab. I. Note that *Archangel* is the first ever UAV-based dataset collection not only containing both real and synthetic data but also providing an extensive set of metadata, including object poses and UAV positions.

### B. UAV-based Object Detection Methods

With the rapid development of generic object detection methods [54] and the aforementioned UAV-based object detection benchmarks (Tab. I), the detection accuracy of UAV-based object detectors has improved significantly over the past few years. In addition to common issues for generic object detection, UAV-based object detection has its own unique challenges [47]. In general, all of the challenges can be roughly divided into three categories. First, objects in UAV-based images are usually much smaller [53]. Therefore, many solutions have been proposed to address this problem to date. For example, [32] proposes a network architecture (HRDNet) that fuses information from both high- and low-resolution

<sup>2</sup>*Archangel* is available for access through: <https://a2i2-archangel.vision>

TABLE I  
COMPARISON OF RECENT UAV-BASED DATASETS. (1K = 1000)

Name		General information						Metadata			
		Tasks	Year	#Clips	#Images	Resolution	Syn/Real	Human category	Human poses	UAV positions	Illumination conditions
Stanford Drone Dataset [38]		TF	2016	60	929.5k	1400x1904	R	✓			
UAV123 [35]		OT	2016	123	112.6k	1280x720	S+R	✓			
Okutama-Action [3]		AD	2017	43	77.4k	3840x2160	R	✓	✓		
CARPK [16]		OC	2017	n/a	1.4k	1280x720	R				
UAVDT [52]		ODT	2018	100	80k	1024x540	R		✓	✓	
VisDrone [56]		ODT	2018	263	179.3k 10k (static)	multiple	R	✓			
DroneSURF [20]		FRD	2019	200	411.5k	1280x720	R	✓			
AU-AIR [6]		OD	2020	8	32.8k	1920x1080	R	✓	✓		
MOR-UAV [33]		MOR	2020	30	10.9k	multiple	R				
DOTA-v2.0 [10]		AOD	2021	n/a	11.3k	multiple	R				
UAV-Human [26]		AR, PE PReID AttrR	2021	67.4k (AR)	22.5k (PE) 41.3k (PReID) 22.3k (AttrR)	1920x1080	R	✓	✓		
SeaDroneSee [45]		ODT	2022	208 (SOT) 22 (MOT)	5.6k (OD) 54.1k (MOT)	multiple	R	✓	✓		
A212-Haze [36]		IER OD	2022	n/a	1k	1845x1500	R	✓	✓		
<i>Archangel</i>	<i>Real</i>	OD	2022	69	41.4k	1304x978	S+R	✓	✓	✓	✓
	<i>Mannequin</i>			598	178.8k	1920x1080					
	<i>Synthetic</i>			n/a	4423.7k	512x512					

Notation	Description	Notation	Description	Notation	Description	Notation	Description
TF	Trajectory Forecasting	OT	Object Tracking	AD	Action Detection	OD	Object Detection
OC	Object Counting	ODT	Object Detection & Tracking	FRD	Face Recognition & Detection	AR	Action Recognition
PE	Pose Estimation	MOR	Moving Object Recognition	AOD	Aerial Object Detection	PReID	Person Re-identification
AttrR	Attribute Recognition	SOT	Single Object Tracking	MOT	Multiple Object Tracking	IER	Image Enhancement & Restoration

inputs to simultaneously preserve features of small objects and maintain computational costs. Based on a similar idea, [31] also introduces a multi-branch and parallel structure (MPFPN) to extract more powerful features for tiny object detection. Besides the scale of an object, target objects in UAV-based datasets are usually crowded and sparsely distributed, reducing both the accuracy and efficiency of an object detector. Thus, [50] proposes a network (ClusDet) that performs object cluster proposal first before detecting objects. Finally, UAV-based datasets contain many UAV-specific nuisances [48], such as varying UAV altitudes and viewing angles. These nuisances cause tremendous variations in object appearances, causing degraded detection performance. To address this issue, [48] proposes to adopt adversarial training to learn domain-robust features from UAV-specific nuisances coarsely annotated by the authors. In this paper, we posit that UAV-based object detection can be further enhanced by providing UAV-based benchmarks with a set of fine-grained metadata, such as that contained in *Archangel*.

In addition to improving the detection accuracy, reducing the computational cost to achieve real-time on-board processing is also very important for UAV-based object detection approaches. One way to improve latency is to skip unnecessary computation. For instance, [2] proposes to extract candidate regions of target objects first via over-segmentation. After that, only windows around the candidate regions are sent to the pre-trained CNN and linear SVM for feature extraction and classification. Another way of reducing computational overhead is to use more efficient one-stage object detectors, such as YOLO [4], [18], RetinaNet [27], CenterNet [12], and EfficientDet [42]. These one-stage object detectors directly classify and locate objects without generating region proposals, resulting in improved latency. As an example, [30] adapts the original network architecture of YOLO by making it more suitable for UAV-based object detection. In this paper, we also utilize

TABLE II  
COMPLEXITY OF THE YOLOV5 MODELS USED IN THIS STUDY. THE RESULTS ARE GENERATED BY [18].

Model	#parameters (M)	FLOPs (G)
<i>YOLOv5n6</i>	3.1	4.3
<i>YOLOv5s6</i>	12.3	16.2
<i>YOLOv5m6</i>	35.3	49.1

*YOLOv5* [18] for all the experiments due to the advantage of its low complexity (Tab. II).

### III. ARCHANGEL DATASET

The data collection process for *Archangel* is illustrated in Fig. 3 and a brief comparison of the three sub-datasets is provided in Tab. III. In the following, we will go through the data collection process of each sub-dataset in detail.

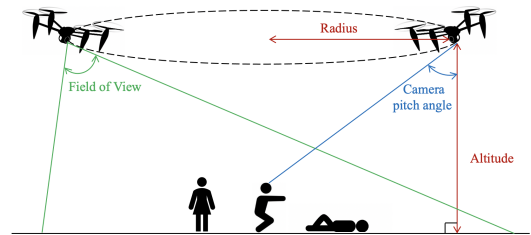


Fig. 3. Illustration of the data collection process for *Archangel*. For each data collection, a number of objects (real people, mannequins, or virtual characters) on the ground were captured by a camera mounted on a UAV (real or simulated). Each of the objects were in one of the three defined poses (*stand*, *kneel*, and *prone*). The UAV circled around the objects at a predefined altitudes and radii of rotation circles.

#### A. *Archangel-Mannequin*

1) *Target Objects*: During this data collection, a group of mannequins were used as human surrogates primarily due to

TABLE III  
COMPARISON OF THE THREE SUB-DATASETS COMPRISING ARCHANGEL.

<i>Archangel</i>	Image Size	Targets	Altitude (m)	Radius (m)	Field of View	Camera Pitch Angle
<i>Synthetic</i>	512×512	Virtual characters	[5-80] increment by 5	[5-80] increment by 5	22.5°	various
<i>Mannequin</i>	1920×1080	Mannequins, vehicles	[15-50] increment by 5	[15-50] increment by 5	120°	45°
<i>Real</i>	1304×978	Real people	[15-50] increment by 5	[20-50] increment by 5	45°	22.5°, 45°, 67.5°

the safety guidelines of the test facility and the difficulty of asking humans to maintain certain strenuous poses, such as *prone* and *squat*, for a long period of time. The mannequins were dressed in casual outfits and positioned in three different poses (*stand*, *kneel*, and *prone*). Hence, the distribution gap between human attributes and those of mannequins' is not noticeably large. Additionally, the dataset also includes a small group of various types of civilian vehicles as targets, such as sports utility vehicles (SUVs), minivans, and sedans. Each target in the dataset was labeled as *mannequin-standing*, *-kneeling*, *-prone* or *civilian vehicles*.

2) *Data Collection*: The imagery was captured using a contractor-built UAV equipped with an onboard electro-optical (EO) camera (ELP-USBFHD01M-L21) with a 1920×1080 pixel array and a lens with approximately 120° field-of-view (FOV). The UAV camera was pitched forward by 45° relative to level flight. During the course of multiple UAV flights, the UAV operated over a wide range of altitudes and radii of rotation circles while keeping the camera pointed inward toward the targets and circling a central point. Both the altitude and radius of the rotation circle were varied from 15-50 meters in 5-meter increments. Since the target objects were stationary and the camera pitch angle was constant, the target objects were spread across different regions of the camera's FOV, resulting in different view angles.

### B. Archangel-Synthetic

1) *Motivation*: While *Archangel-Mannequin* provides valuable aerial imagery with pose and position metadata well suited for UAV-based human detection, the imaging conditions of this data collection were limited. Furthermore, *Archangel-Mannequin* did not incorporate some important factors, such as various human appearances/attributes, extended ranges of UAV altitudes and radii of rotation circles, and different illumination conditions. To overcome these restrictions, a large-scale synthetic imagery (*Archangel-Synthetic*) dataset containing multiple virtual humans in the same poses as that used in *Archangel-Mannequin* was generated using the Unity game engine [19] to augment *Archangel*.

2) *Data Generation and Labeling*: In the Unity-based simulation, a 3D scene is constructed using a terrain asset (background) and one or more target assets (virtual characters in different outfits and poses). For the current version of *Archangel-Synthetic*, we use only a simple terrain model (desert), but we plan to integrate more complex terrain models in future work.

For each target asset, we first created a Unity project and configured the lighting and camera parameters in a virtual 3D environment. A Unity terrain asset (the desert background) and the target asset were then added to the 3D environment.

After the 3D environment was configured as above, a C# script was then used to control the position and viewing angle of the camera as it circled around the target. At each step, the camera was pointed at the center of the target. The script was iterated to encompass the whole range of UAV camera altitudes, the radii of the circles, and the camera viewing angles relative to the target, thus producing imagery captured at various camera-to-target distances and camera pitch angles. Additionally, the sun angle was varied to generate synthetic images captured at different times of a day with corresponding illumination conditions. This resulted in large-scale synthetic imagery with significant target pose, scale, and illumination variations.

To synthesize images and annotations from the virtual 3D environment constructed above, we used an open source software asset, Image Synthesis for Machine Learning [43]. Specifically, the software produces an image segmentation mask where each target object in a synthetic image is assigned a unique scalar value. To generate the bounding box annotations for each target, a Python script was used to parse each segmentation mask, identify each target object, and measure the center, width, and height of the tightest bounding box encompassing the target. Additionally, the target category, the camera position, the target orientation relative to the camera, the camera-to-target distance, the camera pitch angle, and the number of pixels inside the segmentation mask are recorded in a single JavaScript Object Notation (JSON) file for each trial.

3) *Properties*: *Archangel-Synthetic* includes mountainous desert terrain and eight different virtual characters, each in three different poses (*stand*, *squat*, and *prone*). In a single trial of synthetic data generation (a virtual character with a certain pose), both the altitude of the camera and the radius of the rotation circle were varied from 5-80 meters in 5-meter increments. Additionally, the camera viewing angle relative to the character was varied from 0°-358° in 2° increments and four different sun angles were simulated. This resulted in over 4.4M images included in *Archangel-Synthetic*. Each image contains 512×512 pixels with horizontal and vertical fields-of-view of 22.5°.

### C. Archangel-Real

1) *System Design*: The dataset was collected with an ARL-designed UAV platform called the Dawn Dove (D2). The D2 is a re-configurable UAV, with the ability to shift the center of gravity by adjusting arm angles, arm placement, battery, sensor payload, and on-board processor location. It is composed of a combination of 3D printed polyethylene terephthalate glycol (PETG) and carbon fiber infused nylon, and traditional carbon fiber parts. It can carry various types of sensor payloads and on-board processors. It has an approximate payload capacity

of 1.5 lbs and an approximate flight time of 8 minutes. For this data collection, the sensor payload consisted of a UI-3250ML-C-HQ EO camera with an Edmund Optics 6mm/F1.4 lens and a FLIR Boson 640 8.7 mm IR camera. The cameras were co-located on the front of the D2 and the EO camera’s image was cropped to match the FOV of the FLIR Boson (50° HFOV). The on-board processor was an NVIDIA Xavier NX with a 1 TB NVMe SSD for additional data storage.

2) *Data Collection*: In this dataset, the targets consisted of real people wearing civilian clothing in three different poses: *stand*, *kneel*, and *prone*. The data collection process involved having the D2 fly circles at radii ranging from 20-50 meters, at intervals of 5 meters, and at altitudes ranging from 15-50 meters, at intervals of 5 meters. The camera angle relative to level flight was manually adjusted between flights from  $-22.5^\circ$ ,  $-45^\circ$ , and  $-67.5^\circ$  to ensure the targets remained within the FOV of the cameras. In total, 52 circles were flown around the targets. To fly the circles, custom Robot Operating System (ROS) based autonomy code was used, along with a custom Python-based graphical user interface (GUI), which communicated with the UAV. From the ground control station (GCS), the target GPS location, circle radius, altitude, maximum velocity, and file name were entered into the GUI. Once the circle parameters were entered, the D2 was manually armed, launched, and then switched over to “offboard mode” which passed control of the UAV to the GCS. The GCS then commanded the UAV to perform the autonomous circle. Once complete, the next circle’s parameters were entered into the GUI and sent to the UAV while still in the air. This was repeated each flight until the UAV had to be brought back down to replace the battery. In addition to stationary targets, a few circles were also flown where the people walked, jogged, crawled, and waved.

#### D. Importance of the Camera Parameters

Before moving on to the data analysis section, we want to highlight the importance of revealing the camera parameters used in the data collection. Note that the scale of human instances in UAV-based object detection datasets, such as *Archangel*, is strongly influenced by the camera parameters used in the data collection, including FOV, pixel-array size, and pitch angles, in addition to the UAV altitude and radius of rotation circle. Hence, the detection results can vary greatly when using different camera parameters. However, all the conclusions derived from the following data analysis of *Archangel* can still be applied to other UAV-based datasets using different camera parameters through extrapolation. That is, the performance gap can be easily calibrated by adjusting the scale of human instances if the camera parameters and the original object size are known *a priori*.

## IV. DATA ANALYSIS

### A. Overview

In this paper, we design a series of experiments based on the flow shown in Fig. 4. In brief, for each experiment, we select one of the three pre-trained YOLOv5 models (Tab. II) and fine-tune the model on varying amounts of UAV-based real

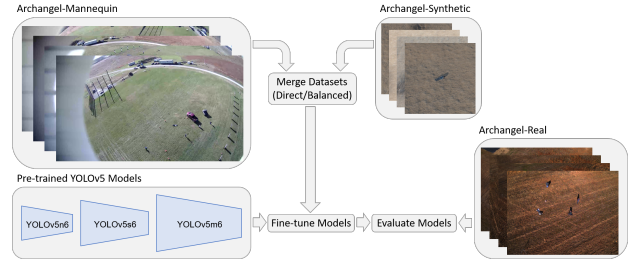


Fig. 4. Overview of the designed experimental flow. The pre-trained YOLOv5 models with various complexity are fine-tuned on different hybrid sets of UAV-based real and synthetic data and evaluated on a hold-out UAV-based dataset.

(Archangel-Mannequin) and synthetic (Archangel-Synthetic) data. We then evaluate the model on a sequestered UAV-based dataset (Archangel-Real). Based on the experimental results, the designed experimental flow can provide valuable insights into optimizing UAV-based object detectors with hybrid sets of real and synthetic data.

### B. Datasets

Note that acquiring the best performance for an UAV-based object detector is not the primary purpose of this study. Thus, we subsample each of the three sub-datasets of *Archangel* to explore optimal strategies for fine-tuning or evaluating models:

- 1) *Archangel-Mannequin*: The dataset consists of video clips collected in 11 UAV flight trials. In this paper, we carefully split the dataset into two subsets so that each covers the whole range of the UAV positions covered during the entire data collection. The video clips collected in 6 of the 11 trials (Trial-5, 6, 8, 9, 10, 11) are used for evaluating models. The rest (from Trial-1, 2, 3, 4, 7) are used for fine-tuning models. All the video clips are uniformly subsampled at 3 fps. This results in two sets of frames, *Arch-Mann-FT37*, containing 6.7k frames for fine-tuning models, and *Arch-Mann-Eval*, containing 11.2k frames for evaluating models. *Arch-Mann-FT37* is named based on the amount of data it has compared to the entire *Archangel-Mannequin* in terms of percentage (37%).
- 2) *Archangel-Real*: Similarly, we uniformly subsampled the video clips in *Archangel-Real* at 1 fps. This results in a set of frames, named as *Arch-Real-Eval*, which containing 4.1k frames for evaluating models.
- 3) *Archangel-Synthetic*: Only one virtual character in all of the three poses is used. For each UAV position, only one of the four sun angles is randomly selected. Additionally, instead of using all the UAV positions, we uniformly sampled images across each rotation circle in  $60^\circ$  increments. This results in a set of images, named as *Arch-Syn-FT*, containing 4.6k images for fine-tuning models.

Each of the three sub-datasets has its own unique usage in this study. In general, *Archangel-Real* serves as the primary UAV-based benchmark for measuring detection accuracy. *Archangel-Mannequin* can be viewed as the real UAV-based

fine-tuning dataset for adapting the detection models to the target UAV-based domain. Although it includes mannequins instead of real humans, fine-tuning on this dataset is shown to be effective in the following sections. *Archangel-Synthetic*, on the other hand, is used as the synthetic version of the UAV-based fine-tuning dataset, which can be combined with *Archangel-Mannequin* to further optimize the models.

### C. Evaluation

We utilize standard AP50, the average precision with an IOU (Intersection of Union) threshold of 0.5, as the metric to measure the performance of each object detector. Moreover, AP50 is computed for each pose respectively. As more than one pose may exist in a single image, to obtain the performance for only one certain pose, the other two poses are ignored during the evaluation process.

### D. Implementation Details

The official repository of YOLOv5 [18] is used for both fine-tuning and evaluating models. The input images are rescaled (imgsz=1280) first before being fed into all the models. During fine-tuning, the backbone for each model is frozen (freeze=10) to prevent the model from easily overfitting. We fine-tune each model for 20 epochs with a batch size of 16 on a server with 4 NVIDIA GeForce RTX 2080 TI GPUs. During the evaluation, we set the confidence threshold to be 0.05. If not specified otherwise, the default settings are adopted.

### E. Experimental Results

1) *Pre-training on MS-COCO [28]*: To begin with, we evaluate the three pre-trained YOLOv5 models on *Arch-Mann-Eval* and *Arch-Real-Eval*. The results are shown in Fig. 5. From the results, we can gain several useful insights on UAV-based object detection.

First, larger pre-trained models achieve better accuracy across all the evaluation datasets and poses. One possible reason for this is that larger models, compared with smaller ones, can explore better and find more powerful features for classification and detection [7]. Although it implies that we can get higher accuracy by using larger pre-trained models, such larger models may not fit well on small UAV platforms with computational constraints.

Another trend we can observe is that the pre-trained models have much better accuracy on *stand*. It is mainly because that the dataset used for pre-training models (MS-COCO) contains significantly more human instances in *stand* (84.53%) [17]. In other words, it is impractical to directly use detectors pre-trained on standard datasets, especially in unusual scenarios where we need to detect people in uncommon positions, such as search and rescue in disaster relief.

It is worth mentioning that the pre-trained YOLOv5 models perform much worse on *Arch-Mann-Eval* than on *Arch-Real-Eval*. That is mainly because *Arch-Mann-Eval* contains some other objects, such as traffic cones and fiducials, which are easily misclassified as humans when captured by the pre-trained detectors at high altitudes [25].

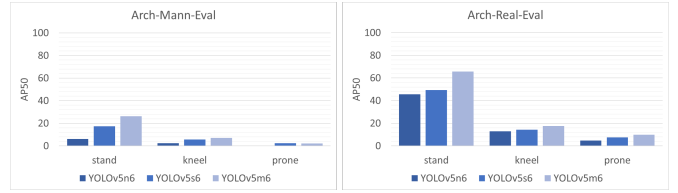


Fig. 5. AP50 of the pre-trained YOLOv5 models evaluated on *Arch-Mann-Eval* and *Arch-Real-Eval*.

2) *Fine-tuning on Arch-Mann-FT37*: As we have discussed, most ground-based datasets used to fine-tune models usually lack UAV-specific samples for the models to learn from, such as human instances in non-standing positions captured from various camera viewing angles and altitudes. Therefore, in this section, we allow the pre-trained YOLOv5 models to acquire such knowledge by fine-tuning the models on *Arch-Mann-FT37*.

Moreover, given the significant challenges of collecting and annotating UAV-based datasets [56] and the lack of existing large-scale UAV-based object detection benchmarks, we explore the idea of fine-tuning models in the small-data regime [5]. More precisely, we subsample the original fine-tuning dataset and create several subsets for fine-tuning, which contain much less data (*Arch-Mann-FT20*, *Arch-Mann-FT10*, *Arch-Mann-FT5*, and *Arch-Mann-FT2*). We follow the same naming strategy as *Arch-Mann-FT37* for the extra fine-tuning datasets.

The results are presented in Fig. 6. Most importantly, we want to highlight the importance of having an evaluation dataset with different characteristics from the fine-tuning dataset. As we fine-tune the models on data from *Arch-Mann-FT37*, we can improve their detection accuracy more on a similar evaluation dataset such as *Arch-Mann-Eval*. However, if the models are fine-tuned on too much data from *Arch-Mann-37FT*, their detection accuracy on *Arch-Real-Eval* tends to drop. We argue that that is because the models start to learn certain dataset-specific features from the fine-tuning dataset, adversely affecting the models' generalization capability to unseen datasets, such as the evaluation dataset in our case.

In practice, ML models embedded into UAVs are usually deployed to new environments unseen during training. Thus, in the following experiments, we choose to fine-tune models on data from *Arch-Mann-FT37* and *Arch-Syn-FT* but evaluate them on *Arch-Real-Eval*.

3) *Fine-tuning on Arch-Mann-FT37 and Arch-Syn-FT*: One of the significant advantages of *Archangel* is that it contains both real and synthetic subsets acquired from similar imaging conditions in data collections and synthetic rendering, respectively. Hence, investigating the effect of augmenting the original UAV-based fine-tuning datasets with UAV-based synthetic data is another major topic for this study. To do so, we fine-tune the pre-trained YOLOv5 models on *Arch-Syn-FT*. Additionally, a well-known concern about learning from synthetic data is that, compared with real data, synthetic data usually contains much less variations in appearances/attributes of objects or structures of scenes [39]. Therefore, instead of fine-tuning models only on *Arch-Syn-FT*, we also explore

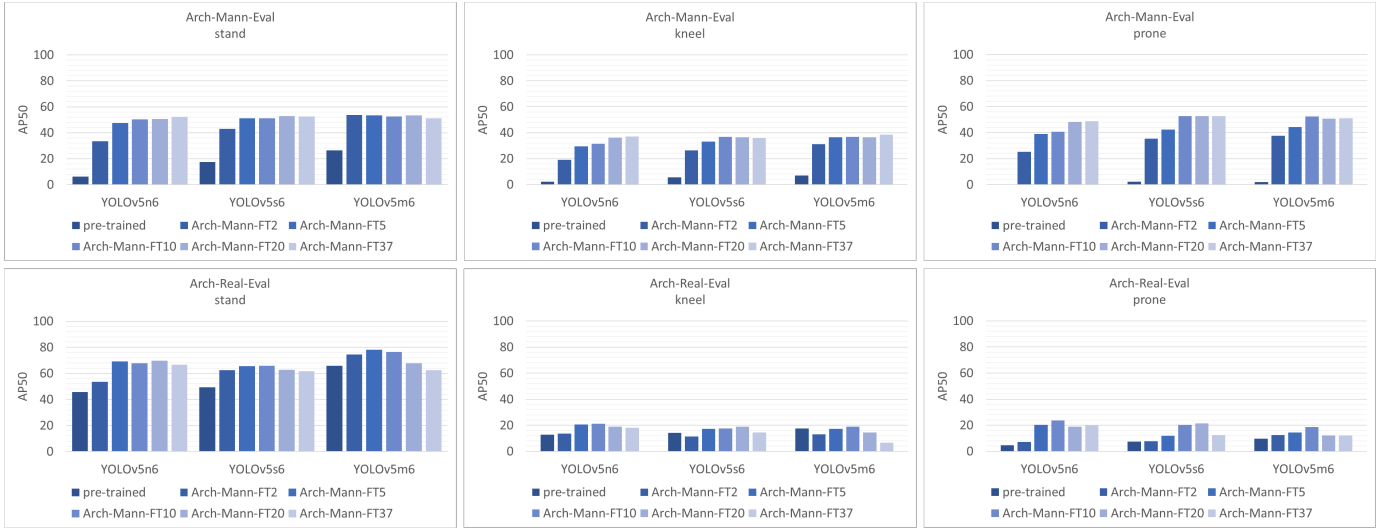


Fig. 6. AP50 of the YOLOv5 models fine-tuned on the different subsets of *Arch-Mann-FT37*. Each model is evaluated on *Arch-Mann-Eval* (top) and *Arch-Real-Eval* (bottom).

the idea of multi-source learning [55], constructing multiple hybrid fine-tuning datasets by directly merging *Arch-Syn-FT* with all the subsets of *Arch-Mann-FT37* (Sec. IV-E2).

The results are shown in Fig. 7. For *prone*, a rarely seen pose in the pre-training dataset, it is indicated that the detection accuracy of the pre-trained models is very low. After fine-tuning the models on the various hybrid subsets of *Arch-Syn-FT* and *Arch-Mann-FT37*, the detection accuracy continually increases with few exceptions. For *stand*, the pre-trained models perform much better than they do for *prone* as expected, but fine-tuning on the hybrid sets of the real and synthetic data still provides much improvement over the pre-trained models, as clearly observed from the detection accuracy of *YOLOv5n6*. Similar observations can be made for *kneel*.

We now compare the results shown in Fig. 6 with the ones shown in Fig. 7 to highlight the effect of adding the synthetic data to the fine-tuning dataset based only on the subsets of *Arch-Mann-FT37*. The results are shown in Fig. 8. For *prone*, we can observe significant performance improvement across all the models and hybrid subsets for fine-tuning after introducing the synthetic data into the fine-tuning datasets, compared with the results of fine-tuning on data from *Arch-Mann-FT37* only. One explanation for the above finding is that most of the human instances in the pre-training dataset are in certain upright positions, including *stand* and *kneel*. Therefore, adding synthetic characters in *prone* captured from various camera viewing angles and UAV altitudes to the fine-tuning dataset can effectively aid the models to learn how to detect humans in *prone*. More in-depth analysis of this issue is discussed in Sec. V-B.

Additionally, *Arch-Syn-FT*, which includes only one virtual character and one type of background, might be too simple for larger models, such as *YOLOv5s6* and *YOLOv5m6* in our case, to learn from, causing them to overfit to the fine-tuning dataset. A proof of this assumption is that using *Arch-Syn-FT* along with the subsets of *Arch-Mann-FT37* to fine-tune *YOLOv5s6* and *YOLOv5m6* significantly decreases their performance on

*stand* and *kneel*, especially when we include fewer data from *Archangel-Mann-FT37* (Fig. 8). On the other hand, fine-tuning *YOLOv5n6* on *Arch-Syn-FT* along with the subsets of *Arch-Mann-FT37* does not have such a negative effect. As a result, in the following ablation study, we focus on analyzing the results of *YOLOv5n6* once we include *Arch-Syn-FT* in the fine-tuning dataset.

## V. ABLATION STUDY

### A. Adjusting the Size of *Arch-Syn-FT*

We have demonstrated the effects of directly combining the various subsets of *Arch-Mann-FT37* with the same set of synthetic data (*Arch-Syn-FT*) for fine-tuning models (Fig. 7 and 8). In this section, we are interested in further exploring the outcome of using different amounts of synthetic data to fine-tune models. Notably, we aim to investigate whether a “balanced” fine-tuning dataset, which contains the same amount of real and synthetic data, is better than its “unbalanced” counterpart, in which the ratio of the synthetic data to the real data varies due to the use of a fixed set of the synthetic data across all the hybrid fine-tuning datasets.

To achieve this goal, for each real fine-tuning dataset (*Arch-Mann-FT37*, *Arch-Mann-FT20*, *Arch-Mann-FT10*, *Arch-Mann-FT5*, and *Arch-Mann-FT2*), the corresponding amount of data is randomly sampled from *Arch-Syn-FT* to match the real fine-tuning dataset. Namely, if the real fine-tuning dataset is smaller than *Arch-Syn-FT*, a subset of *Arch-Syn-FT* is randomly selected and combined with the real fine-tuning dataset to form a balanced fine-tuning dataset. Similarly, if the real fine-tuning dataset is larger, a random subset of *Arch-Syn-FT* is duplicated before the combination. We denote the synthetic fine-tuning dataset as *Arch-Syn-FT-B* if the aforementioned data balancing procedure has been conducted.

The results are shown in Fig. 9, 10 and 11. Comparing Fig. 8 with Fig. 10, we can observe that the negative effect of fine-tuning larger models (*YOLOv5s6* and *YOLOv5m6*) on

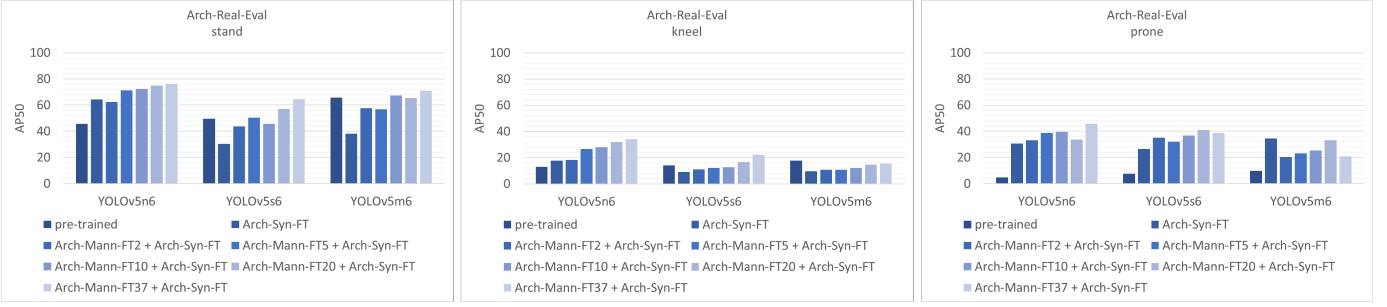


Fig. 7. AP50 of the YOLOv5 models fine-tuned on the various hybrid sets constructed by *Arch-Syn-FT* and the different subsets of *Arch-Mann-FT37*.

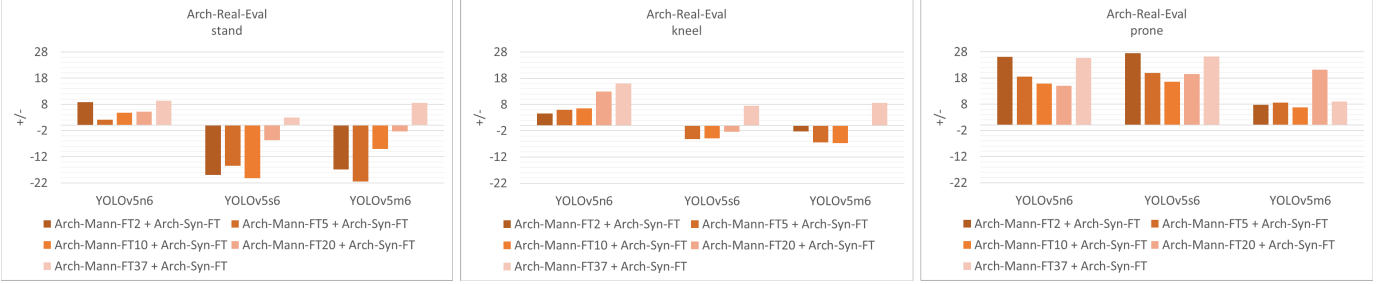


Fig. 8. AP50 improvement of the YOLOv5 models after adding *Arch-Syn-FT* to the original fine-tuning datasets based on the different subsets of *Arch-Mann-FT37*.

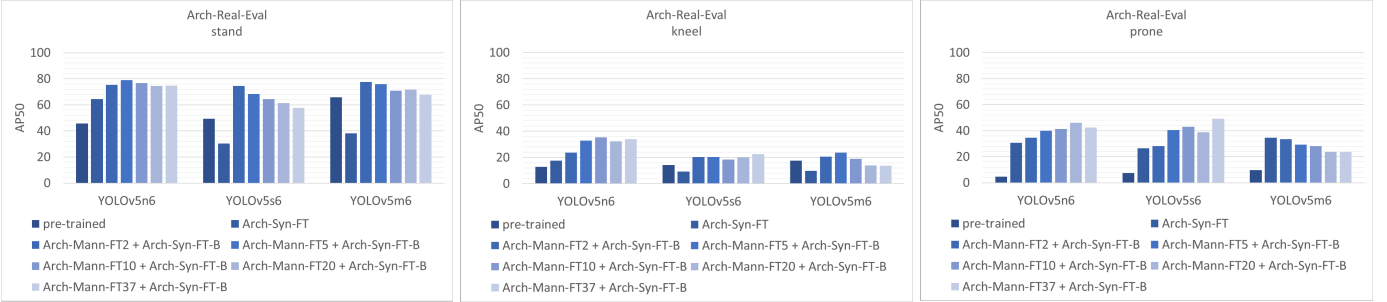


Fig. 9. AP50 of the YOLOv5 models fine-tuned on the various balanced hybrid sets constructed by *Arch-Syn-FT-B* and the different subsets of *Arch-Mann-FT37*.

hybrid fine-tuning sets (Sec. IV-E3) has largely decreased or even diminished. Moreover, the improvement becomes more significant, especially for *YOLOv5n6*. From Fig. 11, it is shown that fine-tuning *YOLOv5n6* on the balanced hybrid sets of the real and synthetic data can always be at least on par with the best performance setting for fine-tuning. These findings indicate that the proportion of each data to the whole fine-tuning dataset significantly impacts the model's fine-tuning performance.

### B. Leaving One Pose Out from Arch-Syn-FT

We have claimed in Sec. IV-E3 that fine-tuning models with synthetic human instances are particularly important for *prone*, a pose rarely seen in the original training data. In this section, we would like to provide more evidence to support this statement.

We use *YOLOv5n6* for this set of experiments since it shows less sign of overfitting when fine-tuning on *Arch-Syn-FT* (Fig. 7). Additionally, the technique of dataset balancing (Sec. V-A) is adopted due to its positive effect on fine-tuning

models (Fig. 9 and 10). More specifically, we follow a similar procedure (Sec. V-A) to generate each hybrid fine-tuning dataset, except that each time one of the poses, *stand*, *kneel*, or *prone*, is excluded in advance from *Arch-Syn-FT*, resulting in a "leave-one-pose-out" fine-tuning dataset, *Arch-Syn-FT-NoSt*, *Arch-Syn-FT-NoKn*, or *Arch-Syn-FT-NoPr*, respectively.

The results are presented in Fig. 12. In general, the detection accuracy of *stand* and *kneel* does not obviously change when we remove any one of the poses from the synthetic fine-tuning dataset. However, the performance of *prone* degrades drastically when we exclude the virtual characters in *prone* from the fine-tuning dataset, which strongly support our earlier claim (Sec. IV-E3).

### C. Performance Comparison on the Altitude/Radius Grid

So far, we have demonstrated that the detection accuracy of the pre-trained YOLOv5 models on the UAV-based evaluation dataset can be considerably boosted by fine-tuning the models on the hybrid sets of UAV-based real and synthetic data. For example, we have shown that the AP50 of the pre-trained

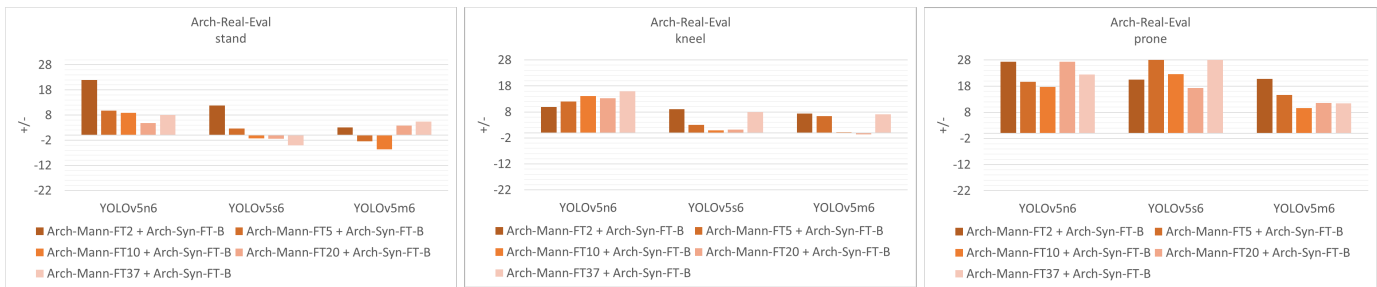


Fig. 10. AP50 improvement of the YOLOv5 models after adding *Arch-Syn-FT-B* to the original fine-tuning datasets based on the different subsets of *Arch-Mann-FT37*.

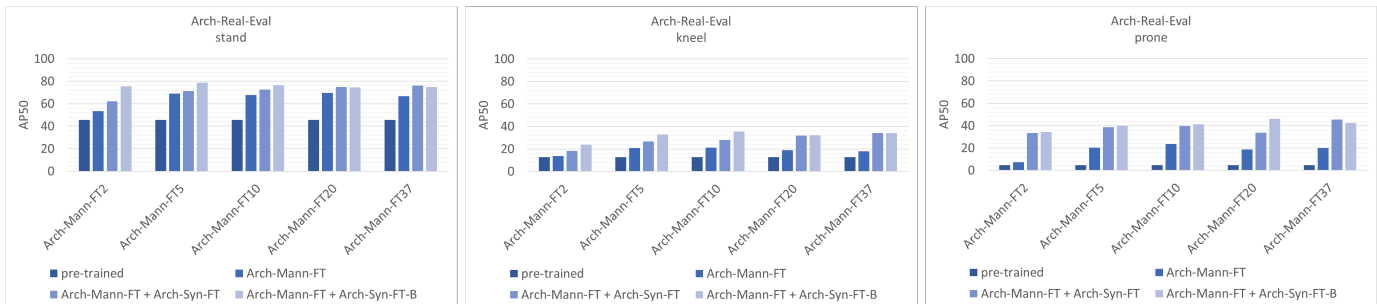


Fig. 11. AP50 comparison of *YOLOv5n6* fine-tuned on the different hybrid sets of *Arch-Syn-FT*, *Arch-Syn-FT-B*, and the different subsets of *Arch-Mann-FT37*.

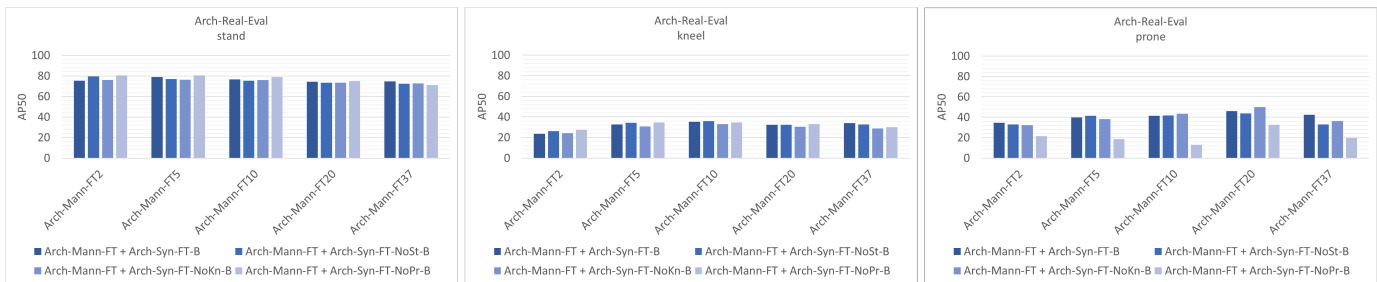


Fig. 12. AP50 of *YOLOv5n6* fine-tuned on the various balanced hybrid sets constructed by the three leave-one-pose-out synthetic fine-tuning datasets (*Arch-Syn-FT-NoSt-B*, *Arch-Syn-FT-NoKn-B*, and *Arch-Syn-FT-NoPr-B*) and the different subsets of *Arch-Mann-FT37*.

*YOLOv5n6* can be increased by about 30 in AP value by fine-tuning it on a joint set of *Arch-Mann-FT2* and *Arch-Syn-FT-B* (Fig. 11). In this section, we further analyze this particular example with the complete information about the UAV positions over the altitude/radius grid as shown in Fig. 13. Our goal is to give an idea of how to utilize the metadata provided by *Archangel* to diagnose problems with a UAV-based object detection model.

The results are presented in Fig. 13. In this figure, we can clearly observe how the pre-trained *YOLOv5n6*'s performance gradually progresses with the different fine-tuning datasets, from the real-data-only dataset to the unbalanced hybrid dataset to the balanced hybrid dataset. Initially, the pre-trained *YOLOv5n6* performs fairly well at the low altitudes but fails at the high altitudes due to the curse of the pre-training dataset, which is composed mostly of ground-based human instances. After being fine-tuned on *Arch-Mann-FT2*, the fine-tuned *YOLOv5n6* gets much better at detecting human instances from a relatively higher altitude or larger circle radii. However, the detection accuracy of the human instances at close range

decreases considerably. We argue that this is mainly because the image resolution of *Arch-Mann-FT2* (1920x1080) is much larger than that of the evaluation dataset (1304x978) and the bounding boxes contained in *Arch-Mann-FT2* are generally small. In other words, fine-tuning *YOLOv5n6* on *Arch-Mann-FT2* inevitably causes a bias on the model toward detecting tiny objects. In contrast, this negative effect does not occur when we fine-tune the model on the hybrid set of *Arch-Mann-FT2* and *Arch-Syn-FT* (or *Arch-Syn-FT-B*). We believe that this is because our synthetic dataset covers an extended range of UAV positions over the grid so as to cause less bias on the fine-tuning process.

Based on the results shown in Fig. 13, to further improve the model's detection accuracy, we can focus on improving the model's performance at high altitudes and large circle radii, or the performance of non-standing positions, such as *kneel* and *prone*. Notably, we find that the performance improvement of *kneel* is surprisingly small to high altitudes and large circle radii, which requires a deeper investigation in future work.

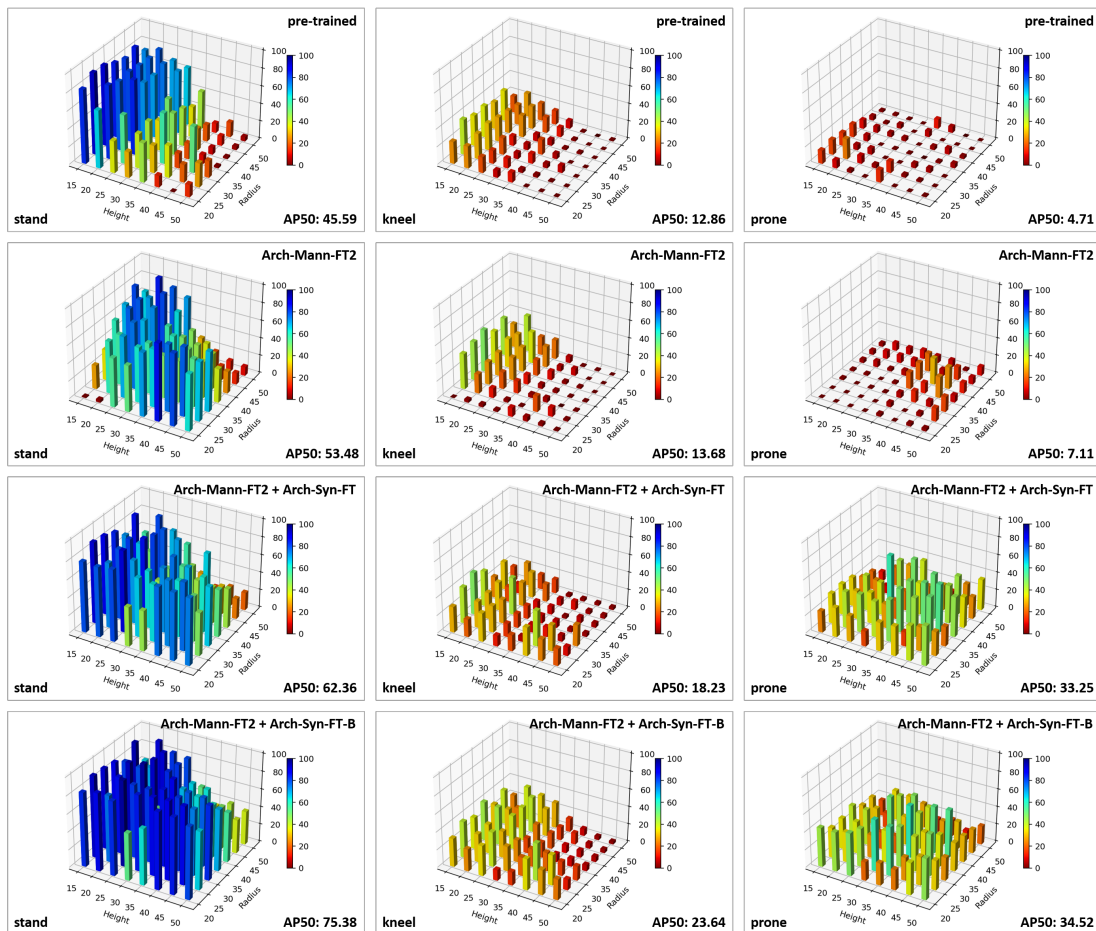


Fig. 13. AP50 comparison on the altitude/radius grid of *YOLOv5n6* fine-tuned on the different hybrid sets of *Arch-Mann-FT2*, *Arch-Syn-FT* and *Arch-Syn-FT-B*.

## VI. DISCUSSION AND FUTURE DIRECTION

With the series of experiments presented in Sec. IV and V, we have demonstrated the distinctive value of the *Archangel* dataset. Particularly, we have clearly illustrated how to utilize the dataset’s metadata to evaluate and diagnose the UAV-based object detectors on the altitude/radius grid. Moreover, we have systematically analyzed how to involve both real and synthetic data within the UAV-based fine-tuning process. Such fundamental studies of UAV-based perception had not been achieved until we curated *Archangel*.

Despite having all these merits, *Archangel* is still in its early stage and has much room for improvement and development. In the following, we suggest a few possible future directions regarding *Archangel*:

### A. Direct Extension of this Study

Many results shown in Sec. IV and V imply that increasing the data diversity of *Archangel* is one of the most promising future research directions. For instance, since we have demonstrated that fine-tuning models with virtual characters in unusual poses are particularly effective (Sec. V-B), we can include more atypical poses into *Archangel* to further explore this phenomenon, which is crucial especially in search and rescue scenarios where finding people in severe physiological

states is the priority. Additionally, we can diversify the appearances/attributes of either the real or synthetic human instances in the dataset, investigating whether this will resolve the issue of overfitting as we have discussed earlier (Sec. IV-E3). For the same purpose, we can increase the diversity of components beyond the foreground objects, such as the real and synthetic backgrounds included in *Archangel*. Finally, we can extend *Archangel* to include more object categories, such as various types of vehicles, which frequently exist in other UAV-based object detection datasets (Tab. I) so that *Archangel* can be used in conjunction with those datasets.

Next, exploring more sophisticated fine-tuning strategies is another potential direction to extend this work. In this study, we have demonstrated that the performance of the pre-trained state-of-the-art object detector can be boosted considerably by fine-tuning the model on a balanced UAV-based fine-tuning dataset constructed by directly merging a real subset and a synthetic subset (Sec. V-A). Nevertheless, it is worth exploring if there is a better strategy for sampling each subset or merging the two subsets. For instance, to build up a balanced fine-tuning dataset, instead of randomly selected samples from the synthetic fine-tuning dataset, we may do the sampling based on certain distance measurements.

### B. UAV-based Visual Representation Learning with Metadata

In this study, we use the position and pose metadata provided by *Archangel* only for accurate model evaluation and diagnosis. However, we believe that there is a huge potential to utilize such metadata during training for better visual representation learning. A notable example for this is NDFT [48], where the authors exploit adversarial training with the coarse metadata labeled by themselves to enhance the robustness of the learned features for UAV-based object detection. We expect that such a framework will benefit greatly from the extensive metadata provided by *Archangel*. Beyond UAV-based perception, in medical [46] and underwater [49] imaging, it has also been shown that dataset metadata is useful for learning visual representation with self-supervised learning or contrastive learning.

### C. UAV-based Synthetic Data Generation and Augmentation

In Sec. IV-E3, we have found that fine-tuning larger models with the synthetic data that we generated often causes the issue of overfitting. This issue might be mitigated by directly synthesizing more diverse images (Sec. VI-A). However, as we have discussed in Sec. IV-E3, there is usually a huge domain gap between the synthetic data and real data in terms of object appearances/attributes and scene structures, which may not be solved by simply increasing the number of synthetic images. Hence, addressing this domain gap issue within the scope of UAV-based perception is another important future research direction for *Archangel*. Possible solutions include: (1) jointly training an object detector with a generative model which transforms synthetic images to be more visually realistic [29], and (2) formulating the process of synthetic data generation as a learning problem to synthesize scene structures better matching real-world scene distributions [21].

## VII. CONCLUSION

In this paper, we introduce a unique UAV-based object detection dataset, *Archangel*, to encourage the community to continue developing more effective UAV-based object detection approaches with dataset metadata and synthetic data. A comprehensive study is carefully designed to show how to utilize *Archangel* to fully optimize a state-of-the-art object detector with a hybrid fine-tuning dataset comprising both real and synthetic data. Additionally, we also demonstrate the huge benefit of leveraging the dataset metadata during model evaluation by comparing the performance of the model across the different object poses and UAV positions. As we have discussed, although there is still much room for improvement, we hope that *Archangel* is useful for the broader machine learning community and can lead to future advances in the area of UAV-based perception.

## VIII. ACKNOWLEDGMENT

This research was sponsored by the Defense Threat Reduction Agency (DTRA) and the DEVCOM Army Research Laboratory (ARL) under Grant No. W911NF2120076. The authors would like to thank the US Army Artificial Innovation Institute (A2I2) for supporting the annotation of *Archangel*.

## REFERENCES

- [1] H. Snoussi A. Chriki, H. Touati and F. Kamoun. Uav-based surveillance system: an anomaly detection approach. In *Proceedings of IEEE Symposium on Computers and Communications*, pages 1–6, 2020.
- [2] Nassim Ammour, Haikel Alhichri, Yakoub Bazi, Bilel Benjdira, Naif Alajlan, and Mansour Zuair. Deep learning approach for car detection in UAV imagery. *Remote Sensing*, 9(4):312, 2017.
- [3] Mohammadamin Barekatin, Miquel Martí, Hsueh-Fu Shih, Samuel Murray, Kotaro Nakayama, Yutaka Matsuo, and Helmut Prendinger. Okutama-action: An aerial view video dataset for concurrent human action detection. In *2017 IEEE Conference on Computer Vision and Pattern Recognition Workshops (CVPRW)*, pages 2153–2160, 2017.
- [4] Alexey Bochkovskiy, Chien-Yao Wang, and Hong-Yuan Mark Liao. Yolov4: Optimal speed and accuracy of object detection. *arXiv preprint arXiv:2004.10934*, 2020.
- [5] Jorg Bornschein, Francesco Visin, and Simon Osindero. Small data, big decisions: Model selection in the small-data regime. In *International conference on machine learning*, pages 1035–1044. PMLR, 2020.
- [6] Ilker Bozcan and Erdal Kayacan. Au-air: A multi-modal unmanned aerial vehicle dataset for low altitude traffic surveillance. In *2020 IEEE International Conference on Robotics and Automation (ICRA)*, pages 8504–8510. IEEE, 2020.
- [7] Alon Brutzkus and Amir Globerson. Why do larger models generalize better? a theoretical perspective via the xor problem. In *International Conference on Machine Learning*, pages 822–830. PMLR, 2019.
- [8] Yaru Cao, Zhijian He, Lujia Wang, Wenguan Wang, Yixuan Yuan, Dingwen Zhang, Jinglin Zhang, Pengfei Zhu, Luc Van Gool, Junwei Han, et al. Visdrone-det2021: The vision meets drone object detection challenge results. In *Proceedings of the IEEE/CVF International Conference on Computer Vision*, pages 2847–2854, 2021.
- [9] Jia Deng, Wei Dong, Socher Richard, Li-Jia Li, Kai Li, and Li Fei-Fei. Imagenet: A large-scale hierarchical image database. In *2009 IEEE/CVF Conference on Computer Vision and Pattern Recognition (CVPR)*, 2009.
- [10] Jian Ding, Nan Xue, Gui-Song Xia, Xiang Bai, Wen Yang, Michael Yang, Serge Belongie, Jiebo Luo, Mihai Datcu, Marcello Pelillo, et al. Object detection in aerial images: A large-scale benchmark and challenges. *IEEE transactions on pattern analysis and machine intelligence*, 2021.
- [11] Piotr Dollár, Christian Wojek, Bernt Schiele, and Pietro Perona. Pedestrian detection: A benchmark. In *2009 IEEE conference on computer vision and pattern recognition*, pages 304–311. IEEE, 2009.
- [12] Kaiwen Duan, Song Bai, Lingxi Xie, Honggang Qi, Qingming Huang, and Qi Tian. Centernet: Keypoint triplets for object detection. In *2019 IEEE/CVF International Conference on Computer Vision (ICCV)*, pages 6568–6577, 2019.
- [13] Milan Erdelj and Enrico Natalizio. UAV-assisted disaster management: Applications and open issues. In *2016 International Conference on Computing, Networking and Communications (ICNC)*, pages 1–5, 2016.
- [14] Mark Everingham, SM Eslami, Luc Van Gool, Christopher KI Williams, John Winn, and Andrew Zisserman. The pascal visual object classes challenge: A retrospective. *International journal of computer vision*, 111(1):98–136, 2015.
- [15] Andreas Geiger, Philip Lenz, and Raquel Urtasun. Are we ready for autonomous driving? the kitti vision benchmark suite. In *2012 IEEE conference on computer vision and pattern recognition*, pages 3354–3361. IEEE, 2012.
- [16] Meng-Ru Hsieh, Yen-Liang Lin, and Winston H Hsu. Drone-based object counting by spatially regularized regional proposal network. In *Proceedings of the IEEE international conference on computer vision*, pages 4145–4153, 2017.
- [17] Ying Huang, Bin Sun, Haipeng Kan, Jiankai Zhuang, and Zengchang Qin. Followmeup sports: New benchmark for 2d human keypoint recognition. In *Chinese Conference on Pattern Recognition and Computer Vision (PRCV)*, pages 110–121. Springer, 2019.
- [18] Glenn Jocher, Ayush Chaurasia, Alex Stoken, Jirka Borovec, NanoCode012, Yonghye Kwon, TaoXie, Jiacong Fang, imyhxy, Kalen Michael, Lorna, Abhiram V, Diego Montes, Jebastin Nadar, Laughing, tkianai, yxNONG, Piotr Skalski, Zhiqiang Wang, Adam Hogan, Cristi Fati, Lorenzo Mammana, Alex Wang1900, Deep Patel, Ding Yiwei, Felix You, Jan Hajek, Laurentiu Diaconu, and Mai Thanh Minh. ultralytics/yolov5: v6.1 - tensorrt, tensorflow edge tpu and opencv export and inference, Feb 2022.
- [19] Arthur Juliani, Vincent-Pierre Berges, Ervin Teng, Andrew Cohen, Jonathan Harper, Chris Elion, Chris Goy, Yuan Gao, Hunter Henry, Marwan Mattar, et al. Unity: A general platform for intelligent agents. *arXiv preprint arXiv:1809.02627*, 2018.

- [20] Isha Kalra, Maneet Singh, Shruti Nagpal, Richa Singh, Mayank Vatsa, and PB Sujit. Dronesurf: Benchmark dataset for drone-based face recognition. In *2019 14th IEEE International Conference on Automatic Face & Gesture Recognition (FG 2019)*, pages 1–7. IEEE, 2019.
- [21] Amlan Kar, Aayush Prakash, Ming-Yu Liu, Eric Cameracci, Justin Yuan, Matt Rusiniak, David Acuna, Antonio Torralba, and Sanja Fidler. Meta-sim: Learning to generate synthetic datasets. In *Proceedings of the IEEE/CVF International Conference on Computer Vision*, pages 4551–4560, 2019.
- [22] Muhammad Arsalan Khan, Wim Ectors, Tom Bellemans, Yassine Ruichek, Davy Janssens, Geert Wets, et al. Unmanned aerial vehicle-based traffic analysis: A case study to analyze traffic streams at urban roundabouts. *Procedia computer science*, 130:636–643, 2018.
- [23] Alina Kuznetsova, Hassan Rom, Neil Aldrin, Jasper Uijlings, Ivan Krasin, Jordi Pont-Tuset, Shahab Kamali, Stefan Popov, Matteo Mallocci, Alexander Kolesnikov, Tom Duerig, and Vittorio Ferrari. The open images dataset v4: Unified image classification, object detection, and visual relationship detection at scale. *IJCV*, 2020.
- [24] Eung-Joo Lee, Damon M Conover, Shuvra S Bhattacharyya, Heesung Kwon, Jason Hill, and Kenneth Evensen. Validation of object detection in UAV-based images using synthetic data. In *Artificial Intelligence and Machine Learning for Multi-Domain Operations Applications III*, volume 11746, pages 584–601. SPIE, 2021.
- [25] Yaesop Lee, Eung-Joo Lee, Damon M Conover, Yi-Ting Shen, Heesung Kwon, Shuvra S Bhattacharyya, Jason Hill, Kenneth Evensen, and G Jeremy Leong. Archangel dataset: UAV-based imagery with position and pose metadata. In *Artificial Intelligence and Machine Learning for Multi-Domain Operations Applications IV*, volume 12113, pages 544–557. SPIE, 2022.
- [26] Tianjiao Li, Jun Liu, Wei Zhang, Yun Ni, Wenqian Wang, and Zhiheng Li. UAV-human: A large benchmark for human behavior understanding with unmanned aerial vehicles. In *Proceedings of the IEEE/CVF conference on computer vision and pattern recognition*, pages 16266–16275, 2021.
- [27] Tsung-Yi Lin, Priya Goyal, Ross Girshick, Kaiming He, and Piotr Dollár. Focal loss for dense object detection. *IEEE Transactions on Pattern Analysis and Machine Intelligence*, 42(2):318–327, 2020.
- [28] Tsung-Yi Lin, Michael Maire, Serge Belongie, James Hays, Pietro Perona, Deva Ramanan, Piotr Dollár, and C Lawrence Zitnick. Microsoft coco: Common objects in context. In *European conference on computer vision*, pages 740–755. Springer, 2014.
- [29] Lanlan Liu, Michael Muelly, Jia Deng, Tomas Pfister, and Li-Jia Li. Generative modeling for small-data object detection. In *Proceedings of the IEEE/CVF International Conference on Computer Vision*, pages 6073–6081, 2019.
- [30] Mingjie Liu, Xianhao Wang, Anjian Zhou, Xiuyuan Fu, Yiwei Ma, and Changhao Piao. UAV-YOLO: Small object detection on unmanned aerial vehicle perspective. *Sensors*, 20(8):2238, 2020.
- [31] Yingjie Liu, Fengbao Yang, and Peng Hu. Small-object detection in UAV-captured images via multi-branch parallel feature pyramid networks. *IEEE access*, 8:145740–145750, 2020.
- [32] Ziming Liu, Guangyu Gao, Lin Sun, and Zhiyuan Fang. Hrdnet: high-resolution detection network for small objects. In *2021 IEEE International Conference on Multimedia and Expo (ICME)*, pages 1–6. IEEE, 2021.
- [33] Murari Mandal, Lav Kush Kumar, and Santosh Kumar Vipparthi. MOR-UAV: A benchmark dataset and baselines for moving object recognition in UAV videos. In *Proceedings of the 28th ACM International Conference on Multimedia*, pages 2626–2635, 2020.
- [34] Hamid Menouar, Ismail Guvenc, Kemal Akkaya, A Selcuk Uluagac, Abdullah Kadri, and Adem Tuncer. UAV-enabled intelligent transportation systems for the smart city: Applications and challenges. *IEEE Communications Magazine*, 55(3):22–28, 2017.
- [35] Matthias Mueller, Neil Smith, and Bernard Ghanem. A benchmark and simulator for UAV tracking. In *European conference on computer vision*, pages 445–461. Springer, 2016.
- [36] Priya Narayanan, Xin Hu, Zhenyu Wu, Matthew D Thielke, John G Rogers, Andre V Harrison, John A D’Agostino, James D Brown, Long P Quang, James R Uplinger, et al. A multi-purpose real haze benchmark with quantifiable haze levels and ground truth. *arXiv preprint arXiv:2206.06427*, 2022.
- [37] Sergey I Nikolenko. *Synthetic data for deep learning*, volume 174. Springer, 2021.
- [38] Alexandre Robicquet, Amir Sadeghian, Alexandre Alahi, and Silvio Savarese. Learning social etiquette: Human trajectory understanding in crowded scenes. In *European conference on computer vision*, pages 549–565. Springer, 2016.
- [39] Viktor Seib, Benjamin Lange, and Stefan Wirtz. Mixing real and synthetic data to enhance neural network training—a review of current approaches. *arXiv preprint arXiv:2007.08781*, 2020.
- [40] Shuai Shao, Zeming Li, Tianyuan Zhang, Chao Peng, Gang Yu, Xiangyu Zhang, Jing Li, and Jian Sun. Objects365: A large-scale, high-quality dataset for object detection. In *Proceedings of the IEEE/CVF international conference on computer vision*, pages 8430–8439, 2019.
- [41] Pei Sun, Henrik Kretzschmar, Xerxes Dotiwalla, Aurelien Chouard, Vijaysai Patnaik, Paul Tsui, James Guo, Yin Zhou, Yuning Chai, Benjamin Caine, et al. Scalability in perception for autonomous driving: Waymo open dataset. In *Proceedings of the IEEE/CVF conference on computer vision and pattern recognition*, pages 2446–2454, 2020.
- [42] Mingxing Tan, Ruoming Pang, and Quoc V. Le. Efficientdet: Scalable and efficient object detection. In *2020 IEEE/CVF Conference on Computer Vision and Pattern Recognition (CVPR)*, pages 10778–10787, 2020.
- [43] U3DC. MI-imagesynthesis, 2017.
- [44] *ug<sup>2</sup>* prize challenge. <http://cvpr2022.UG2challenge.org/index.html>. Accessed: 2022-07-25.
- [45] Leon Amadeus Varga, Benjamin Kiefer, Martin Messmer, and Andreas Zell. Seadronesee: A maritime benchmark for detecting humans in open water. In *Proceedings of the IEEE/CVF Winter Conference on Applications of Computer Vision*, pages 2260–2270, 2022.
- [46] Yen Nhi Truong Vu, Richard Wang, Niranjan Balachandar, Can Liu, Andrew Y Ng, and Pranav Rajpurkar. Medaug: Contrastive learning leveraging patient metadata improves representations for chest x-ray interpretation. In *Machine Learning for Healthcare Conference*, pages 755–769. PMLR, 2021.
- [47] Xin Wu, Wei Li, Danfeng Hong, Ran Tao, and Qian Du. Deep learning for unmanned aerial vehicle-based object detection and tracking: a survey. *IEEE Geoscience and Remote Sensing Magazine*, 10(1):91–124, 2021.
- [48] Zhenyu Wu, Karthik Suresh, Priya Narayanan, Hongyu Xu, Heesung Kwon, and Zhangyang Wang. Delving into robust object detection from unmanned aerial vehicles: A deep nuisance disentanglement approach. In *Proceedings of the IEEE/CVF International Conference on Computer Vision*, pages 1201–1210, 2019.
- [49] Takaki Yamada, Miquel Massot-Campos, Adam Prügel-Bennett, Stefan B Williams, Oscar Pizarro, and Blair Thornton. Leveraging metadata in representation learning with georeferenced seafloor imagery. *IEEE Robotics and Automation Letters*, 6(4):7815–7822, 2021.
- [50] Fan Yang, Heng Fan, Peng Chu, Erik Blasch, and Haibin Ling. Clustered object detection in aerial images. In *Proceedings of the IEEE/CVF International Conference on Computer Vision*, pages 8311–8320, 2019.
- [51] Mohammed Yaqot and Brenno C Menezes. Unmanned aerial vehicle (UAV) in precision agriculture: business information technology towards farming as a service. In *2021 1st International Conference on Emerging Smart Technologies and Applications (eSmarTA)*, pages 1–7. IEEE, 2021.
- [52] Hongyang Yu, Guorong Li, Weigang Zhang, Qingming Huang, Dawei Du, Qi Tian, and Nicu Sebe. The unmanned aerial vehicle benchmark: Object detection, tracking and baseline. *International Journal of Computer Vision*, 128(5):1141–1159, 2020.
- [53] Xuehui Yu, Zhenjun Han, Yuqi Gong, Nan Jan, Jian Zhao, Qixiang Ye, Jie Chen, Yuan Feng, Bin Zhang, Xiaodi Wang, et al. The 1st tiny object detection challenge: Methods and results. In *European Conference on Computer Vision*, pages 315–323. Springer, 2020.
- [54] Syed Sahil Abbas Zaidi, Mohammad Samar Ansari, Asra Aslam, Nadia Kanwal, Mamoona Asghar, and Brian Lee. A survey of modern deep learning based object detection models. *Digital Signal Processing*, page 103514, 2022.
- [55] Kaiyang Zhou, Ziwei Liu, Yu Qiao, Tao Xiang, and Chen Change Loy. Domain generalization: A survey. *IEEE Transactions on Pattern Analysis and Machine Intelligence*, 2022.
- [56] Pengfei Zhu, Longyin Wen, Dawei Du, Xiao Bian, Heng Fan, Qinghua Hu, and Haibin Ling. Detection and tracking meet drones challenge. *IEEE Transactions on Pattern Analysis and Machine Intelligence*, pages 1–1, 2021.